ELSEVIER

Polymer 43 (2002) 2737–2746

polymer

www.elsevier.com/locate/polymer

Kinetics of rapid structural changes during heat setting of preoriented PEEK/PEI blend films as followed by spectral birefringence technique

S. Bicakci, M. Cakmak*

College of Polymer Engineering and Polymer Science, Polymer Engineering Institute, University of Akron, Akron, OH 44325-0301, USA

Received 11 September 2001; received in revised form 30 November 2001; accepted 3 December 2001

Abstract

The influence of composition and preorientation on the development of structural hierarchy during heat setting of PEEK/PEI films was investigated using on-line birefringence, and off-line wide-angle and small-angle X-ray scattering, infrared dichroism and thermal analysis techniques. When the PEEK/PEI blends are drawn to deformation levels below the onset of strain hardening, the subsequent heat setting at high temperature starts with a large relaxation process followed by a fast crystallization and a long-term slow structural rearrangement stages. When the films are predrawn beyond a critical structural level (crystallinity and orientation), the initial relaxation stage disappears. This signifies that beyond a critical structural order a long-range physical network, where the nodes consist of crystallized domains and chain—self and cross-entanglements—are formed. This physical network allows the entropy driven shrinkage stresses to be maintained that results in the development of oriented crystalline phase. The addition of non-crystallizable PEI chains was found to retard the formation of this 'network structure' resulting in lower orientation levels. © 2002 Published by Elsevier Science Ltd.

Keywords: PEEK/PEI blend; Birefringence; Crystallinity and orientation

1. Introduction

Heat setting is an important stage in a typical film process where preoriented films are exposed to temperatures where the rate of crystallization is at a maximum. This generally corresponds to midpoint between the cold crystallization and melting temperatures. During the heat setting process, the film is held in the grips of the machine to preserve any orientation developed during drawing as crystallinity and thermal stability increase. The structural rearrangement process takes place quite fast from oriented and 'structured' precursors. It is important to understand this structural evolution during heat setting in order to be able to control resulting material properties. It was the subject of the previous paper to define the morphology of drawn films since this subsequent annealing stage is expected to be highly dependent on the deformation and thermal history imposed during the drawing stage. As a continuation of the previous paper [1], this paper deals with the fundamental understanding of structure development during heat setting of preoriented PEEK/PEI films at different compositions using an automated on-line spectral birefringence measurement technique. Although intensity methods to determine birefringence of flowing media that utilize a single monochromatic light source have been used extensively in the rheo-optics field [2,3] it has not been robust enough to be automated. There have been also activities where more than one wavelength used to determine birefringence [4]. The first suggestion of the use of continuous visible spectrum to determine birefringence was made by Yang [5] followed by Harding [6]. In a series of papers by Pluta [7], Burghardt [8–11], this technique steadily improved over the years [12]. In none of these previous studies was the spectral birefringence technique automated and made into a real time measurement system.

In our group we have been developing rapid on-line detection techniques involving two colors [13–16] that needed some post processing of data after the acquisition. In order to develop a robust and fully automated system we utilized the developments by Yang, Harding, Burghardt and Posthuma given above and developed an extensive analysis system utilizing the principles of spectral birefringence technique and made it fully automated as demonstrated in publications by Serhatkulu and Cakmak [17,18,20,21,22]. This enabled us to follow the very rapid retardation (and thus birefringence measurement) changes that take place in annealing of oriented films under constraint. The system was able to track changes as little as 0.2 s real time indefinitely [19–21]. This technique allows us to determine the

* Corresponding author. Tel.: +1-330-972-6865; fax: +1-330-258-2339.
E-mail address: cakmak@uakron.edu (M. Cakmak).

0032-3861/02/$ - see front matter © 2002 Published by Elsevier Science Ltd.
PII: S0032-3861(02)00020-4

birefringence of film at 0.2-s intervals. Other off-line techniques such as DSC, wide and small angle X-ray diffraction and infrared (IR) dichroism are combined with the spectral birefringence technique in order to gather the crystallinity and the orientation information from the crystalline and amorphous domains of PEEK/PEI blends.

2. Experimental procedures

2.1. Spectrographic birefringence technique

The experimental set-up for this instrument is shown in Fig. 1. The predrawn films were mounted and tensioned on a circular sandwich frame and subsequently inserted into the preheated oven of the spectral birefringence system and the retardation data were obtained at 0.2 s intervals. The light source is a 200 W Xe/Hg white light that provides enough intensity for the detector over a wide wavelength range (420–695 nm). The light is polarized at 45 °C to the machine direction (MD) of the film inside the heating chamber. The polarized light passing through the sample then comes to the analyzer unit. This unit, which has a computer controlled motion ability with the help of a digital I/O board and a data acquisition card (Keithley Metrabyte), has two analyzers next to each other at 45 and −45 °C to the MD of the film. When the light passes through the analyzer at 45°, the detector gets the parallel-polarized intensity information when it passes through the analyzer at −45°, the detector gets the perpendicular-polarized intensity information. The detector system consists of a quartz optical fiber that leads to a grating spectrograph, which in turn spreads the beam and projects the spectrum onto a photodiode array.

Neglecting any dichroism, Mueller matrix analysis reveals the following equations for the light intensity transmitted through a pair of crossed ($\perp$) or parallel ($\parallel$) polarizers with the sample in between [23]:

$$I^{\perp} = \frac{I_0}{2} e^{-2\alpha} \sin^2\left(\frac{\pi \Delta n d}{\lambda}\right) \tag{1}$$

$$I \parallel = \frac{I_0}{2} e^{-2\alpha}\left[1 - \sin^2\left(\frac{\pi \Delta n d}{\lambda}\right)\right] \tag{2}$$

In these equations I_0 is the incident light intensity at a wavelength λ, Δn the birefringence, d the sample thickness, and $e^{-2\alpha}$ is a term that accounts for the attenuation of light due to isotropic absorption or scattering. Normalizing Eq. (1) with the sum of Eqs. (1) and (2) removes the incident light intensity and any light attenuation:

$$N^{\perp} = \frac{I^{\perp}}{I^{\perp} + I \parallel} = \sin^2\left(\frac{\pi \Delta n d}{\lambda}\right) \tag{3}$$

After computing the normalized intensity ($N^{\perp}$), a Fourier transform smoothing procedure is applied. Since the resolution of detector is only 0.5 nm the peak sections of the spectra are further numerically analyzed and interpolated using a second order polynomial fit for exact determination of the location of the maxima and minima. Using the peak positions (maxima or minima) ($x_{\text{peak}}(\lambda_i)$) and the medium positions ($x_{\text{m}}(\lambda_i)$), retardation ($\Gamma(\lambda)$) is calculated as a function of wavelength [24]. The retardation versus wavelength data is then fitted to the Cauchy dispersion relation and birefringence at a specific wavelength (543.5 nm for this study) is found after the thickness, d, of the sample is measured.

$$x_{\text{m}}(\lambda_i) = \frac{x_{\text{peak}}(\lambda_i) + x_{\text{peak}}(\lambda_i + 1)}{2} \tag{4}$$

$$\Gamma(\lambda_i) = \frac{x_{\text{peak}}(\lambda_i)^2}{2[x_{\text{m}}(\lambda_i) - x_{\text{m}}(\lambda_i - 1)]} \tag{5}$$

$$\Delta n(\lambda) d = \Gamma(\lambda) = A + \frac{B}{\lambda^2} \tag{6}$$

In these experiments, the prestretched samples were sandwiched on a metal frame and rapidly inserted into a preheated oven through trap doors with the help of guide rails running along the length of the convection oven. This guide rail/trap door combination design allowed very fast insertion and removal of the already sandwiched samples with no disturbance to the temperature of the preheated oven. After the prescribed length of time the sample is quenched into a quenched bath situated below the oven through a second trap door at the bottom of the oven.

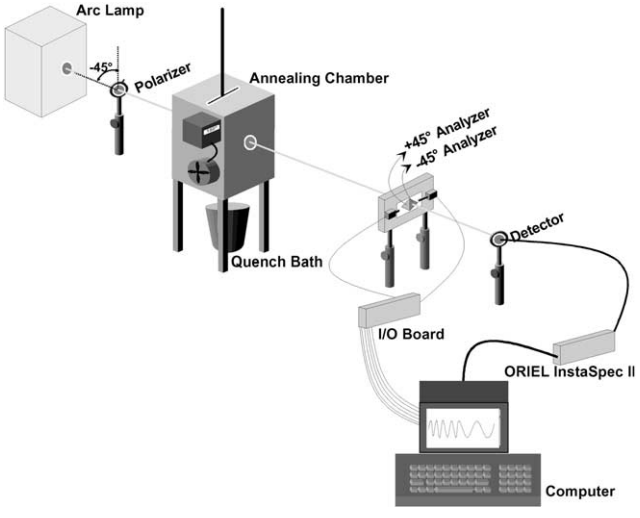

Fig. 1. Spectral birefringence optical set up.

2.2. Determination of orientation

The uniaxial orientation factor of PEEK crystal can be obtained using the Hermans equation [25,26] as generalized by Stein [27]:

$$f_{j,Z} = \frac{3\langle \cos^2(\phi_{j,Z})\rangle - 1}{2} \tag{7}$$

where $\phi_{j,Z}$ is the angle between the j crystallographic axis and the drawing direction Z ($j = a, b, c$). The mean square cosine values of the angle between the crystallographic plane and the reference direction Z can be calculated using

$$\langle \cos^2 \phi_{hkl,Z} \rangle = \frac{\int_0^{\pi/2} I(\phi) \sin \phi \cos^2 \phi \, d\phi}{\int_0^{\pi/2} I(\phi) \sin \phi \, d\phi} \quad (8)$$

where $I(\phi)$ is the diffracted intensity.

The a-axis orientation was directly determined using the (200) plane. The orientation function for the c-axis was indirectly determined by applying Wilchinsky's rule [28,29] to the orientation distributions of the (110) and (200) planes. In the determination of $\langle \cos^2(\phi_{c,Z}) \rangle$ Fratini et al.'s [30] unit cell parameters ($a = 7.83 \pm .02$ Å, $b = 5.94 \pm .01$ Å, $c = 9.86 \pm .04$ Å) were used. The final equation is as follows:

$$\langle \cos^2 \phi_{Z,c} \rangle = 1 - 0.4207 \langle \cos^2 \phi_{Z,200} \rangle - 1.579 \langle \cos^2 \phi_{Z,110} \rangle \quad (9)$$

With f_a and f_c, orientation factor of b-axis was calculated using the orthogonality relation

$$f_a + f_b + f_c = 0 \quad (10)$$

Scattered intensities $I(\phi)$ for (110) and (200) planes were directly obtained from the digital image plate data by the integration of the area in between two circular cuts along the azimuthal direction as shown in Fig. 2. The intensities were corrected by subtracting the amorphous background. The amorphous background was obtained through a circular cut on the WAXS pattern right next to the peak of interest where no crystalline peaks overlap. The amorphous background intensity was corrected by multiplying the intensity values by a normalization factor

$$\mathrm{NF} = I(\theta_1, \chi_1)/I(\theta_2, \chi_1)$$

where θ_1 is the scattering angle from where the crystalline peak is observed, θ_2 the scattering angle where the amorphous background is observed and χ_1 is the azimuthal angle where no crystalline diffraction intensity is observed (here this is about 60°). This process assumes that the azimuthal shape of the anisotropic scattering due to oriented amorphous regions does not change significantly in the range of scattering angles of interest. This procedure is shown in Fig. 2. The corrected intensity data was used in Eq. (8) to obtain the orientation factors. With this method the contributions from the amorphous isotropic and anisotropic regions have been completely eliminated.

2.3. Small angle X-ray scattering

Small angle X-ray scattering (SAXS) measurements were done by Rigaku X-ray generator connected to a 10 m SAXS camera in Oak Ridge National Laboratory. The X-ray machine was operated under 40 kV and 60 mA conditions.

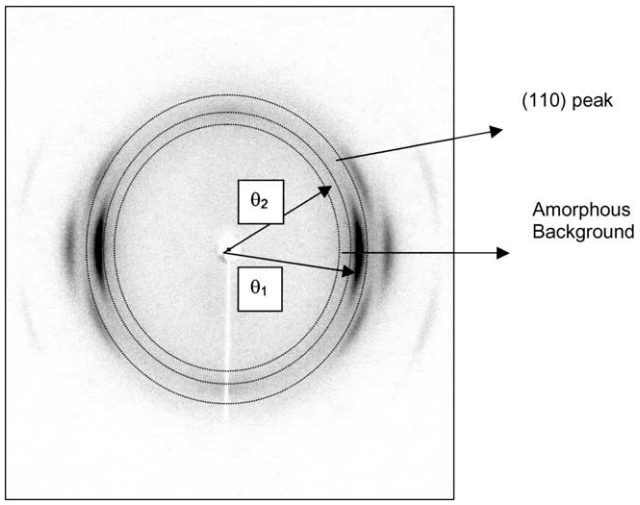

Fig. 2. WAXS measurement procedure.

A 64×64 gas-filled wire detector was used to collect the data. Typical data accumulation time was 20 min for most samples. For samples exhibiting low scattering intensity this accumulation time was extended to improve the counting statistics. The sample to detector distance was 5.119 m. The data was analyzed by a software called spector. The peak position in $I(q)$ versus q plot was used to estimate the Bragg long spacing L_B by Bragg's law. q is defined as $q = (4\pi/\lambda)\sin\theta$, λ and θ being the wavelength and scattering angle of X-ray, respectively. λ and θ are also related by Bragg's law: $\lambda = 2d \sin\theta$. Long spacing is found from $2\pi/q^*$ where q^* is the peak position.

3. Results and discussion

3.1. On-line birefringence during heat-setting of drawn films

Figs. 3 and 4 show the DSC thermograms and the birefringence and normalized crystallinity values of drawn films at different compositions prior to annealing.

The addition of PEI reduces the level of crystallinities (Fig. 4) as well as birefringence levels obtained with deformation primarily as a consequence of spatial dilution of crystallizable PEEK chains despite the stiffening effect of high T_g PEI chains on the stress–strain behavior described in the companion paper [1]. It is of particular note that between 70/30 and 50/50 concentration range the strain induced crystallizability declines sharply.

In order to investigate the kinetics of the structural changes, we chose a 200 °C as the annealing temperature for all compositions as indicated by the vertical dotted line in Fig. 3. With the exception of 50/50 composition this temperature is at or above the cold crystallization peaks where substantial crystallization rates can be achieved.

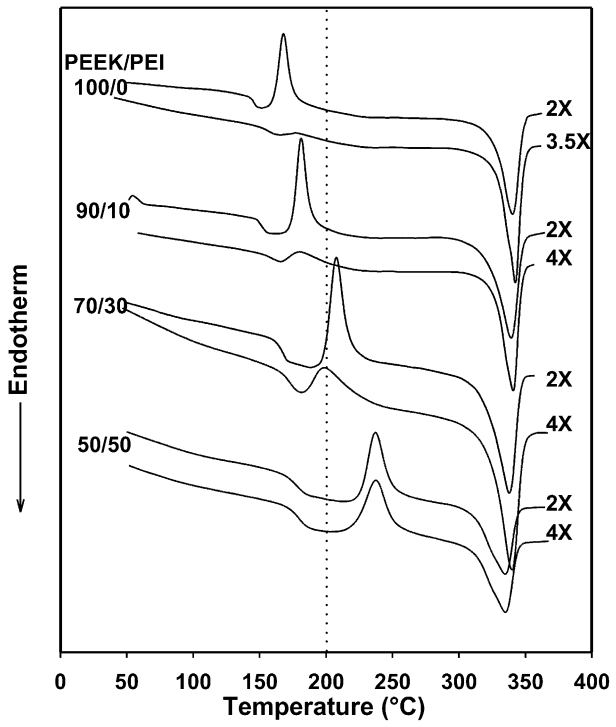

Fig. 3. DSC scans of PEEK/PEI films at different compositions and draw ratios. The dotted line indicates the annealing temperature.

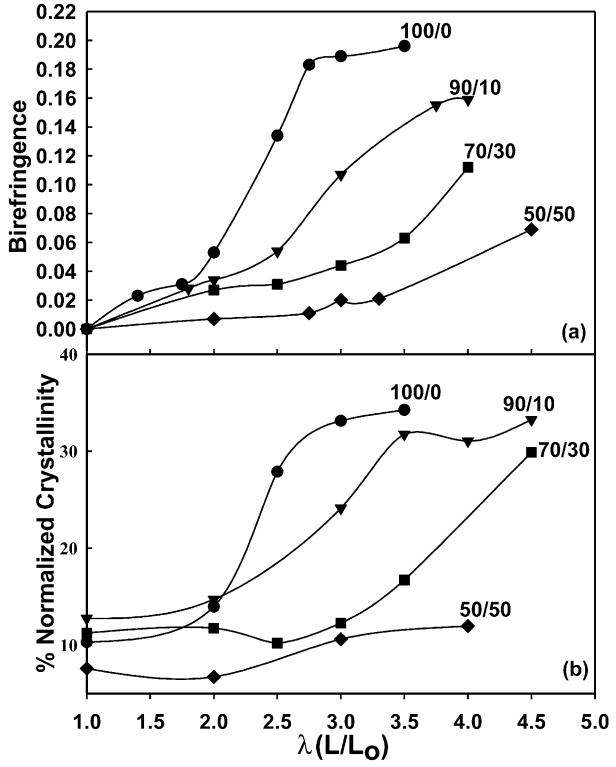

Fig. 4. PEEK/PEI films at different compositions and draw ratios (drawing temperature: T_g + 10 °C): (a) birefringence; (b) % normalized crystallinity.

3.1.1. Time evolution of birefringence during annealing

Figs. 5–9 describe the effect of draw ratio on the development of birefringence with time during annealing of PEEK/PEI films and the resulting kinetics of birefringence change.

As shown in Fig. 5 for neat PEEK, three distinct stages corresponding to different birefringence behavior is observed over the annealing times studied. The earliest stage (IT) is characterized by constant birefringence; this corresponds to the induction period prior to thermal crystallization. A portion of this stage represents non-isothermal conditions as the film is being heated from room temperature to the annealing temperature in a preheated forced convection oven. The short duration stage I where the decrease of birefringence is observed signifies partial relaxation (stage I in Fig. 5) as is evident in 1.5×1 and 2×1 birefringence profiles. In stage II, birefringence increases very rapidly signifying that major structural reorganization takes place over a very short period spanning a few seconds. Stage III is characterized by a slow increase in birefringence values over very long periods. All birefringence profiles in this figure show that birefringence continues to change and does not reach a constant level within 2 h suggesting very slow structural reorganization is occurring over long periods.

With an increase in deformation, the induction time, defined as the clock time between the sample insertion into the preheated oven and the time when the birefringence begins to deviate from initial value, becomes shorter. This is partly as a result of quicker heating due to the decrease in film thickness and partly due to the increase of the rate of

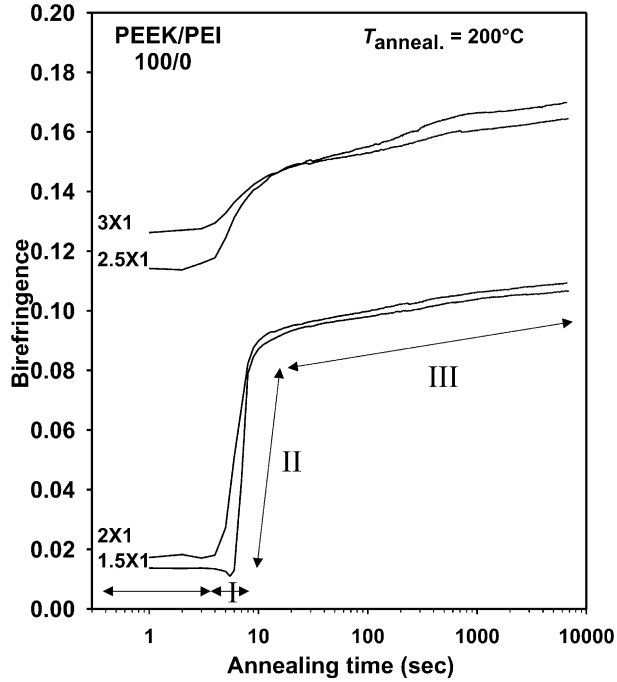

Fig. 5. Effect of draw ratio on the birefringence development of PEEK films annealed at 200 °C.

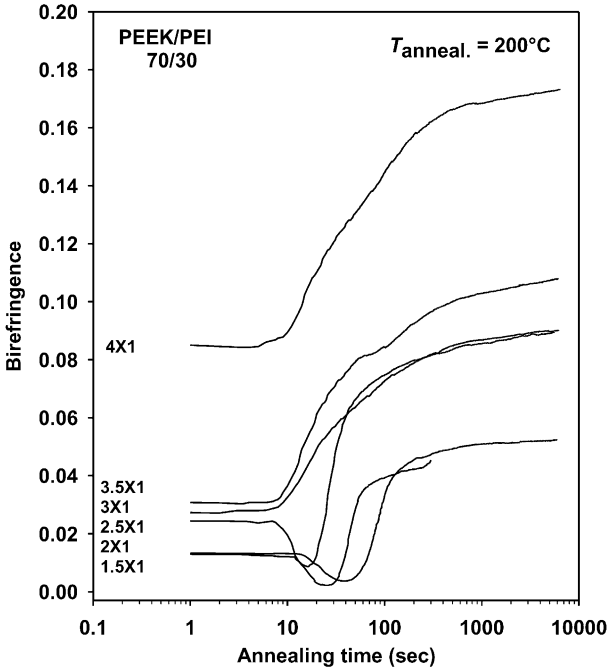

Fig. 6. Effect of draw ratio on the birefringence development of PEEK/PEI (70/30) films annealed at 200 °C.

structural reorientation due to higher levels of preorientation imparted in the stretching stage. As the draw ratio is increased from $\lambda = 2$ to 2.5 there is a significant increase in the initial level of birefringence which is consistent with

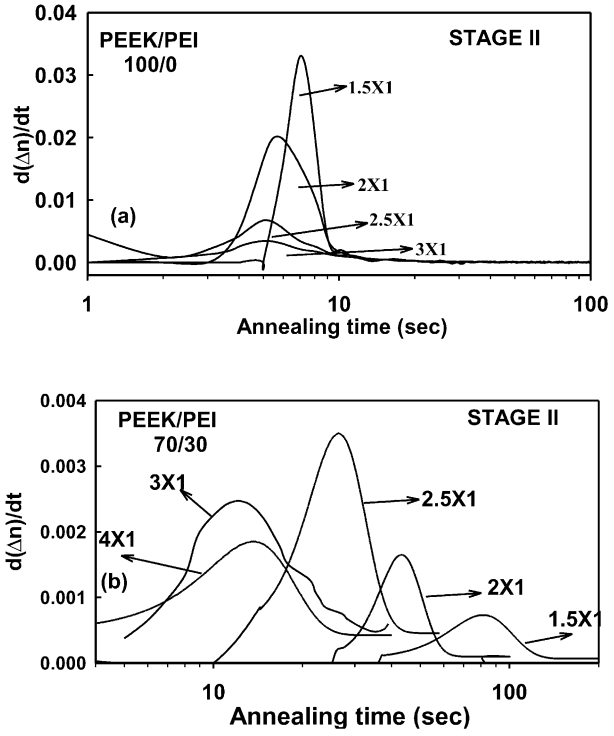

Fig. 7. Temporal variation of time derivatives of birefringence curves of: (a) PEEK.PEI 100/0; (b) PEEK/PEI 70/30.

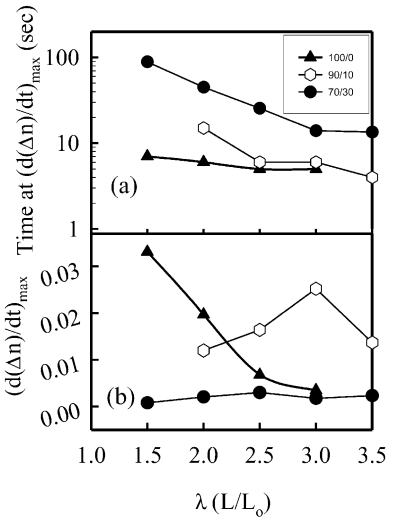

Fig. 8. (a) Time to reach maximum of the time derivative of birefringence curves (Fig. 7); (b) maximum slope of stage II.

the expectations from structure that formed in the drawing stage (also see Fig. 4(a) and (b)). The sharp increase of birefringence accompanied by an increase in crystallinity is a consequence of the formation of a physical network that increases the effectiveness of the drawing process that results in chain extension. In the second stage, the slope of birefringence versus time curve decreases with the increase of draw ratio from 2 to 3 that corresponds to biggest increase in both crystallinity and birefringence shown in Fig. 4(a) and (b). This suggests that the structural hierarchy becomes rather constrained (e.g. 'muscle bound') with increased

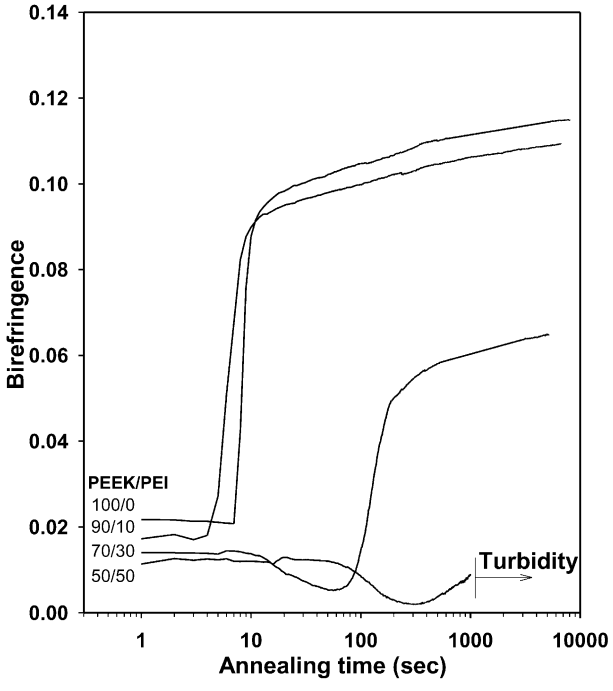

Fig. 9. Effect of composition on the birefringence of 2× drawn PEEK/PEI films annealed at 200 °C.

orientation and crystallinity levels suggesting the formation of 'long-range physical network'.

Upon increase of non-crystallizable PEI fraction to 30%, the relaxation stage I, greatly enlarges in magnitude and duration in films stretched to low to moderate deformation levels (Fig. 6). The time to minimum of stage I becomes shorter with deformation and at 3×1 level this stage I completely disappears. It should be noted that the maximum slope of stage II where the fastest structural reorganization takes place first increases and then subsequently decreases with the increased prestretching. In stage III, the structural rearrangement processes greatly slow down. We have extended these measurements to as long as 24 h and we did not see complete leveling off as these slow processes persist to extended periods.

3.1.1.1. Kinetic parameters. In order to obtain kinetic information, the first time derivatives of Figs. 5 and 6 are shown in Fig. 7 for PEEK/PEI 100/0 and 70/30 as examples. Additionally, time to reach maximum and the value of the maxima are plotted in Fig. 8(a) and (b), respectively. Time to reach the maximum steadily decreases with prestretching levels for all films. Addition of PEI lowers the slope.

What was interesting is the data shown in Fig. 8(b) where the maximum of the first derivative is shown. This parameter is related to the rate constant for the structural process. In the neat PEEK, the maximum is exhibited by the lowest stretch ratio and with deformation this value steadily decreases indicating the rate of change slows down considerably. However, upon addition of 10% PEI we begin to see a maximum (near $3\times$) in these graphs and the same is also true for 70/30 film though it is much less discernible in this scale (near $2.5\times$ also see original data in Fig. 7(b)).

Birefringence values reflect the sum of crystallinity and orientation averaged over the amorphous regions and the crystalline regions. For partially crystallized samples, the overall birefringence is assumed to obey the additivity rule. Neglecting the form birefringence, the total birefringence is defined as

$$\Delta n = \Delta n_{\mathrm{a}} + \Delta n_{\mathrm{c}} = \Delta n_{\mathrm{a}}^{0} f_{\mathrm{a}}(1 - X_{\mathrm{c}}) + \Delta n_{\mathrm{c}}^{0} f_{\mathrm{c}} X_{\mathrm{c}} \qquad (11)$$

where X_{c} is the degree of crystallinity, f the orientation factor, Δn^{0} the intrinsic birefringence and c and a refer to crystalline part and amorphous part, respectively.

According to Eq. (11) the decrease of birefringence during annealing is only possible if there is disorientation of the chains in the amorphous domains or crystalline domains or both. During the annealing process, specific domains of material may be relaxing while others are crystallizing. The decrease in the birefringence level after an induction period is predominantly controlled by long-range relaxations of the oriented molecular chains. This decrease is followed by an increase in birefringence that is predominantly controlled by the crystallization process. This observation reveals that crystallization and relaxation are the two molecular mechanisms occurring simultaneously and govern the annealing behavior of predrawn films.

3.1.1.2. Blend composition effect. The birefringence behavior is greatly influenced by the composition of blends as shown in Fig. 9 for films of varying composition at the same $2\times$ stretch ratio. Addition of PEI significantly expands the relaxation stage I and generally decreases the rates of change in stage II. This is clearly demonstrating that the non-crystallizable PEI chains, though they themselves are rather stiff, do not allow the development of long-range connectivity—we call a network—resulting in greater proportion of the shrinkage forces expended for disorientation of the 'unconstrained' oriented chains. For higher draw ratio samples, the structure is characterized by the presence of a well-developed physical network. As was explained in the companion paper, this network is formed by highly oriented crystallites as well as entanglements acting as nodes and interconnected by taut tie chains. During the annealing of these highly strained films, the presence of this network is believed to prevent long-range relaxations of the chains thereby maintaining or enhancing the overall shrinkage activated stresses that in turn cause further development of oriented crystallization of polymer chain segments. Even though the effect of temperature on the birefringence behavior has not been studied here, one can predict that the relaxation and crystallization mechanisms would be highly dependent on the annealing temperature. It should also be pointed out that the relaxation occurs within very short time scales (20–100 s) and the spectral birefringence technique is able to track the details of these processes.

3.1.2. Time-resolved experiments

As mentioned earlier, birefringence values are a combination of the crystallinity and the orientation information of the polymer chains averaged over amorphous and crystalline domains. In the case of a blend with one crystallizable and one non-crystallizable component, the morphology is extremely complex considering that amorphous phase information is also averaged over the amorphous domains of both components. The phase segregation and resulting formation of additional domains that might occur during annealing will also increase the complexity of the structural hierarchy. Therefore, to understand this behavior, several techniques: DSC, wide and small angle X-ray diffraction, and Fourier transform IR dichroism were combined with the spectral birefringence technique in order to clarify the details of molecular rearrangement processes. For this purpose, 'time-slice' samples were prepared by annealing the drawn films at 200 °C for various time periods followed by rapid quenching in water.

Fig. 10 shows the changes in the crystallinity, birefringence development and thermal properties during annealing of PEEK/PEI (70/30) film with $\lambda = 2$. Three different stages

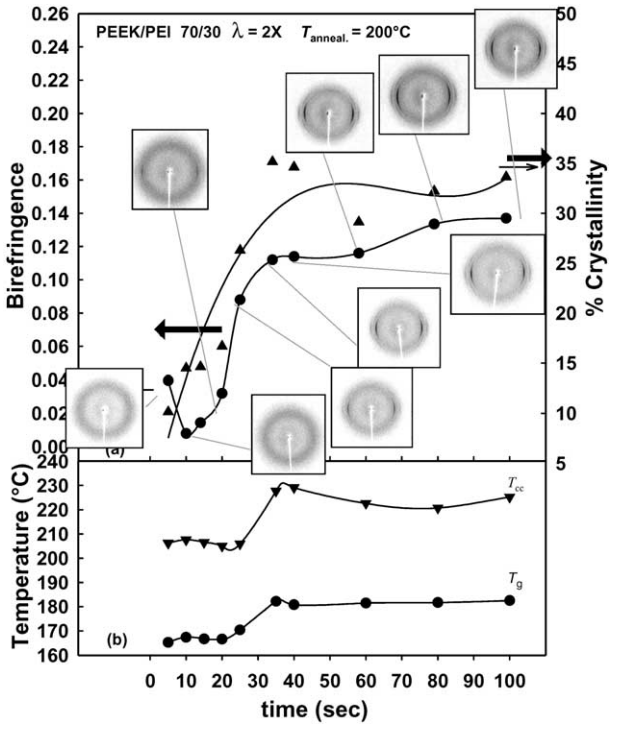

Fig. 10. PEEK/PEI (70/30) films with $\lambda = 2$ annealed at 200 °C: (a) crystallinity and birefringence development; (b) the change of cold crystallization (T_{cc}) and glass transition (T_g) temperature with annealing time.

are observed: the initial birefringence of the drawn film decreases within 10 s and birefringence values approaches zero. The material is amorphous during this period as also indicated by the presence of only the amorphous halo on WAXD patterns. The first sign of crystalline structure is observed in 15 s annealing that also corresponds to the onset of the increase in birefringence. Although birefringence values were quite small at the minimum, crystalline peaks on the equator exhibits a very small azimuthal spread indicating high orientation of the chains in these highly disordered crystalline domains. This behavior reveals that the chains oriented by drawing have not relaxed completely and when sufficient thermal energy was provided to the system, these oriented chains served as precursors for thermal crystallization by overcoming the relaxation process. Naturally the influence of shrinkage forces due to entropic relaxation of oriented amorphous chains should not be neglected particularly if segments of polymer chains are constrained through one of several mechanisms including entanglements, entrapment in small crystalline domains that all contributed to the overall connectivity in the structural hierarchy. This will have a highly localized segmental straightening effect as well while other unconstrained portions are free to relax and randomize.

In the second stage, a very sharp increase in both birefringence and crystallinity is observed. The increase of crystallinity, which restricts the movement of the chains in the amorphous domains, results in an increase of T_g by more than 10 °C. In this 20 s stage, off-equatorial oriented crystalline peaks rapidly emerge in WAXD patterns in parallel with the development of DSC crystallinity indicating this rapid birefringence increase is attributable to oriented crystalline domains. In the third stage, the rate of change in birefringence is significantly decreased compared to the second stage. The crystallinity levels do not change appreciably and T_g and T_{cc} increase little with annealing time. WAXD patterns show that the intensity of the reflections from the crystalline planes increases indicating that there is an enhancement in size/perfection of crystals. However, the overall orientation of the crystals is reduced during annealing as revealed by the increase of the azimuthal broadening of crystalline peaks in this third stage. This decrease of orientation is most likely caused by the crystallization of regions where the disoriented chains reside.

At 4×, the 70/30 blends do not undergo substantial reorganization of molecular structure during annealing (Fig. 11). Crystallinity levels which were close to the maximum achievable crystallinity prior to annealing increased by only 10% at the end of 25 min annealing time and birefringence showed little increase. These slow changes in crystallinity and birefringence are due to the presence of highly constrained structure developed during stretching stage that prevents the long-range relaxation of the chains. It was also observed that both the glass transition temperature increased and the width of the glass transition region increased with time as a result of crystallization. The increase of T_g (mid) as a result of annealing is slightly higher than the increase of T_g (onset). This might indicate that the

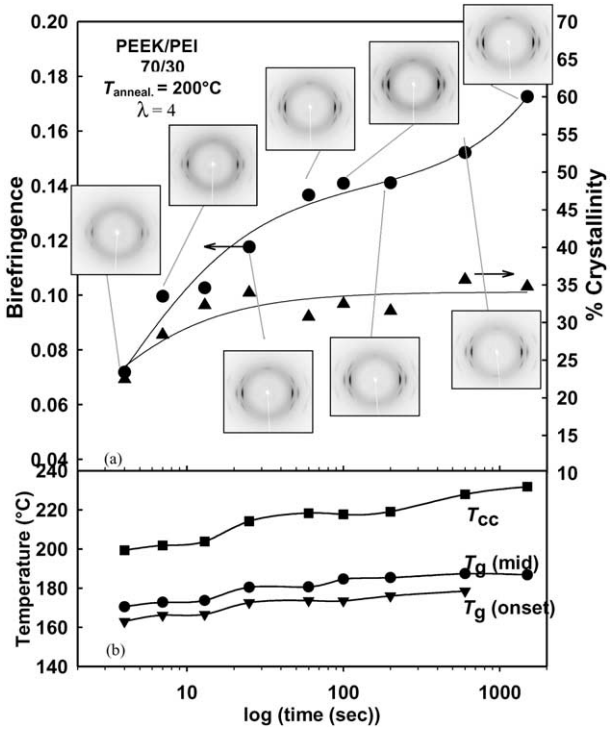

Fig. 11. PEEK/PEI (70/30) film with $\lambda = 4.0$ annealed at 200 °C: (a) crystallinity and birefringence development; (b) the change of cold crystallization (T_{cc}) and glass transition (T_g) temperature with annealing time.

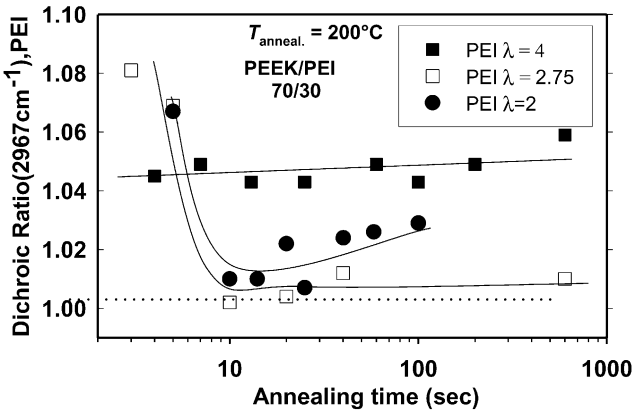

Fig. 12. The variation of the orientation in PEI chains in 2, 2.75 and 4× stretched PEEK/PEI (70/30) with annealing time at 200 °C.

blend phase separation process is driven by the crystallization of PEEK. Indeed, major broadening of T_g was observed by Sauer and Hsiao [31] for PEEK/PEI blends crystallized under quiescent conditions at 260 °C. They stated that the broadening of T_g was the result of the depletion of PEEK from the amorphous phase and the entrapment of PEI into interfibrillar (bundles of lamellae) regions leading to very broad amorphous populations. At the annealing temperature used here, one would expect much lower diffusion rate for PEI.

In order to understand the birefringence behavior, it is important to look more closely at these amorphous domains. Therefore, the IR dichroic ratio of PEI in the blend films was measured. Fig. 12 indicate that the dichroic ratio of 2967 cm^{-1} band of PEI chains is generally low. Annealing brings this to isotropic state within 10 s of start of annealing for both 2 and 2.75× stretched samples. The sample with 4× stretching though exhibiting low dichroic ratio remains constant throughout the annealing perhaps as a result of hindrance of relaxation at such high deformation levels due to the constrained network structure.

The influence of annealing on crystalline orientation factors is shown in Fig. 13. One striking feature of this figure

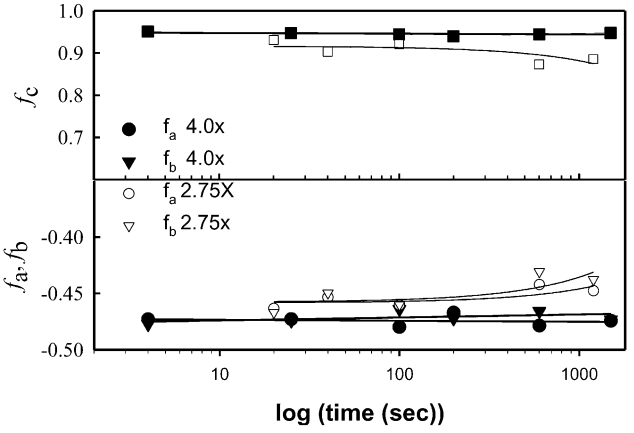

Fig. 13. The change of *a*, *b*, and *c* axes orientations of PEEK crystal during annealing of PEEK/PEI (70/30) film at 200 °C (λ = 2.75 and 4).

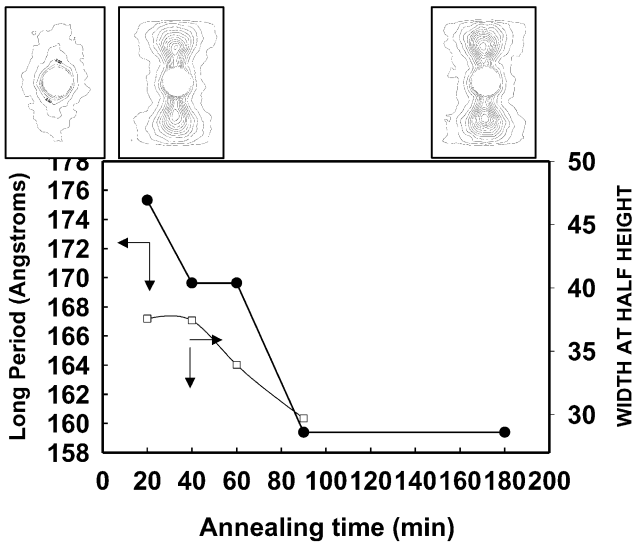

Fig. 14. Long period and width at half height data on PEEK/PEI films annealed at 200 °C.

is that it shows the samples exhibiting near perfect orientation levels in their crystalline regions ($f_c > 0.95$) particularly in the 4× stretched samples. Annealing decreases these values particularly in 2.75× sample in accord with the earlier observations.

In order to gather information about the superstructure of

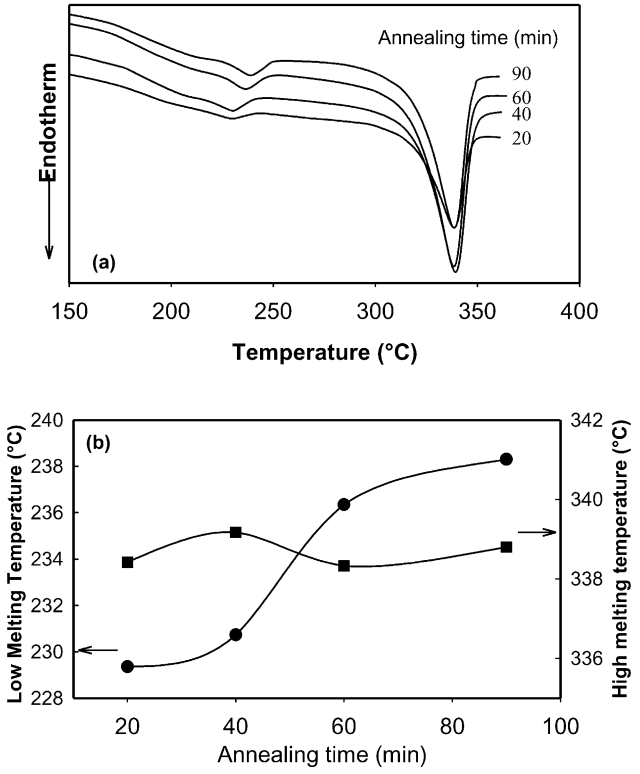

Fig. 15. PEEK/PEI (70/30) (λ = 3) blends annealed at 200 °C: (a) DSC thermograms; (b) the variation of melting temperatures with annealing time.

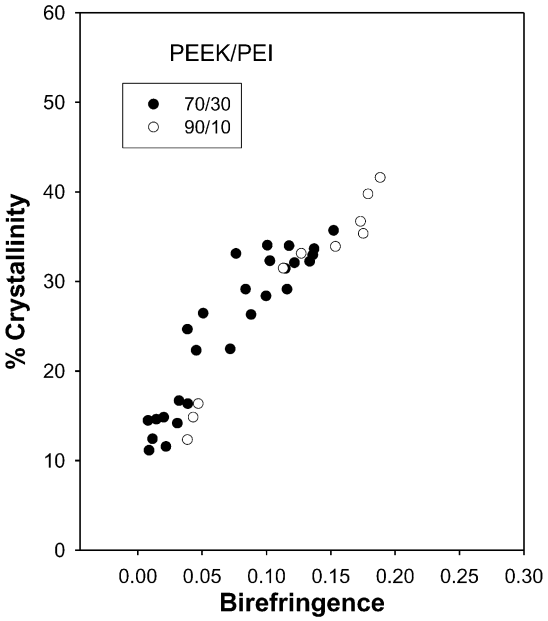

Fig. 16. Crystallinity versus birefringence data for PEEK/PEI blends.

annealed films a set of samples for 70/30 blend with $\lambda = 3$ were analyzed with SAXS. Fig. 14 shows the results. Initial sample does not show any discernible density modulations along the stretching direction as the scattering pattern is ellipsoidal devoid of a discrete maximum. In 20 min discrete scattering maxima emerges and these patterns reveal the existence of a periodic structure with alternating crystalline lamellae and amorphous phase. Long period decreases with annealing time. This can be related to the formation of crystals in the original interlamellar regions with 'insertion' process. The evidence for the insertion crystallization is present in the thermal analysis of these samples shown in Fig. 15. Upon annealing the secondary melting peak emerges about 20 °C above the annealing temperature and increase in area. This peak corresponds to disordered and/or small crystals formed during annealing and these crystals melt at much lower temperatures compared to the primary crystals. The melting temperature and the heat of fusion is found to increase with annealing time indicating that the secondary crystals become more structured with annealing time. This structural rearrangement that takes place slowly is a characteristic of the third stage. On the other hand, T_m of primary crystals is not affected by the annealing process.

Finally, a master graph was obtained by correlating all the crystallinity data to birefringence data (Fig. 16). The graph implies that among the PEEK/PEI blends at the same crystallinity level, the one with higher PEEK content will have higher birefringence.

4. Conclusions

The annealing process of preoriented PEEK/PEI blends

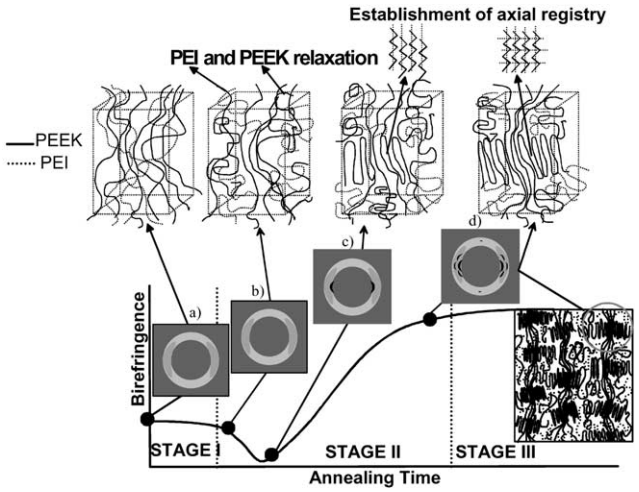

Fig. 17. Proposed mechanism for the annealing of preoriented PEEK/PEI blends at low draw ratio: a, b, c, and d describe the evolution of structure during annealing.

with constrained dimensions was studied at 200 °C. The birefringence time profiles of these blends are greatly influenced by the initial morphology of the drawn blends as determined by the draw ratio, λ and the blend composition. The effect of the annealing process on structure is schematically shown in Figs. 17 and 18.

When the blends with draw ratios below the onset of strain hardening (Fig. 17) are annealed, birefringence decreases after a short induction time (stage I) under the action of entropic shrinkage forces, then recovers and continues to increase at a fast rate (stage II) followed by a very slow stage (stage III). Prior to annealing, these samples are essentially amorphous with unoriented domains and domains where the chains are highly aligned in the drawing direction (Fig. 17(a)). These aligned chains serve as precursors for thermally induced crystallization and form highly extended crystallites. The decrease of birefringence arises

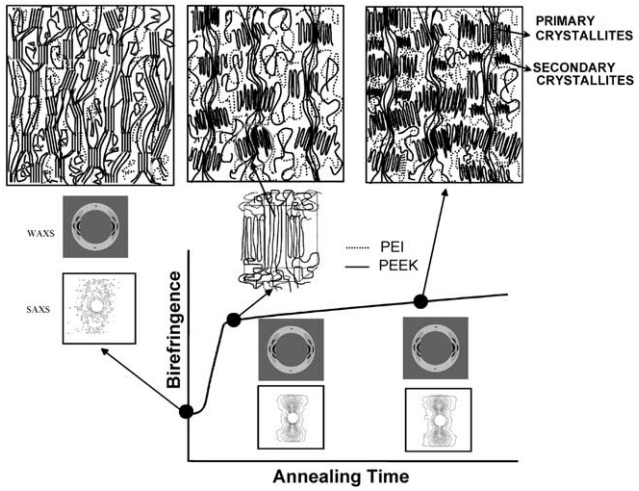

Fig. 18. Proposed mechanism for the annealing of preoriented PEEK/PEI blends at high draw ratio.

from the long-range relaxation of PEI chains and of PEEK chains oriented to a lesser extent than those chains that formed crystallites (Fig. 17(b)). This decrease is followed by an increase in birefringence which is predominantly controlled by effects associated with crystallization. Therefore, the annealing process can be described by two molecular mechanisms occurring simultaneously: relaxation (disorientation) of presumably oriented but 'unanchored' amorphous chains under the action of shrinkage forces and crystallization. During the second stage, major reorganizations take place; birefringence and crystallinity increase rapidly and three-dimensional order, which was absent at the onset of crystallization, develops with time (Fig. 17(c) and (d)). When the crystallinity levels approach 30–35%, the increase of birefringence slows. The perfection of the crystalline structure is improved during this third stage.

The blends with higher draw ratios and above the onset of strain hardening do not show any long-range relaxation (Fig. 18). After a shorter induction time compared to low draw ratio samples, birefringence increases with annealing time through a fast stage followed by a slow stage. In the second region, the change in measured properties is slower when compared to lower draw ratio blends. This behavior of birefringence is related to the existence of a physical network with oriented crystallites together with entanglements acting as nodes and preventing long-range relaxations. The effectiveness of the network in preventing relaxations would largely depend on the existence and concentration of tie molecules connecting the oriented crystallites. A secondary and small crystalline domains are formed and grow with annealing time. Long period is found to decrease indicating secondary smaller crystallites form in the original inter lamellar stacks.

The increase of PEI concentration in the blends was found to retard the formation of the network, the crystallization kinetics and favor the relaxation process.

Acknowledgements

We also would like to thank Mr Toprak Serhatkulu for his assistance in spectral birefringence measurements and Dr J.S. Lin, Baris Yalcin and Jonghan Choi in their help in acquiring the SAXS data at ORNL 10 m camera.

References

[1] Bicakci S, Cakmak M. Polymer 2002;43:149.
[2] Janeschitz-Kriegl H. Polymer melt rheology and flow birefringence. Berlin: Springer, 1983.
[3] Fuller G. Optical rheometry of complex fluids. New York: Oxford University Press, 1995.
[4] Redner AS. Exp Mech 1985:148.
[5] Yang HH, Chouinard MP, Lingg WJ. J Polym Sci, Polym Phys 1982;20:981.
[6] Harding GF. In: Meeten GH, editor. Optical properties of polymers. New York: Elsevier, 1986.
[7] Pluta M. Polymer 1992;33:1553.
[8] Hongladarom K, Burghardt WR, Baek SG, Cementwala S, Magda JJ. Macromolecules 1993;26:772.
[9] Hongladarom K, Burghardt WR. Macromolecules 1993;26:785.
[10] Hongladarom K, Secakusuma V, Burghardt WR. J Rheol 1994;38:1505.
[11] Hongladarom K, Burghardt WR. Macromolecules 1994;27:483.
[12] Beekmans F, Posthuma de Boer A. Macromolecules 1996;29:8726.
[13] Venkatesvaran H, Cakmak M. SPE Antec Tech Pap 1993;39:257.
[14] Venkatesvaran H, Cakmak M. Polym Engng Sci 2001;41:341.
[15] Galay JM, Cakmak M. SPE Antec Tech Pap 1997;43:1606.
[16] Galay JM, Cakmak M. J Polym Sci Phys 2001;39(1):1107.
[17] Serhatkulu T. PhD Dissertation. University of Akron, 2000.
[18] Serhatkulu T, Kokturk G, Cakmak M. SPE Antec Tech Pap 1999;45:1645.
[19] Serhatkulu TF, Cakmak M. SPE Antec Tech Pap 1999:1645.
[20] Kokturk G, Serhatkulu TF, Kozluca A, Piskin E, Cakmak M. SPE Antec Tech Pap 1999;45:2190.
[21] Kokturk G, Serhatkulu TF, Cakmak M. SPE Antec Tech Pap 2000:1737.
[22] Serhatkulu T. PhD Dissertation. University of Akron, 2000.
[23] Hongladarom K, Burghardt WR, Baek SG, Cementwala S, Magda JJ. Macromolecules 1993;26:772.
[24] Beekmans F, de Boer P. Macromolecules 1996;29:8726.
[25] Hermans PH, Platzek P. Kolloid-Z 1939;88:68.
[26] Hermans JJ, Hermans PH, Vermaas D, Weidinger A. Rec Trav Chim Pays-Bas 1946;65:427.
[27] Stein RS. J Polym Sci 1958;31:327.
[28] Wilchinsky ZW. Advances in X-ray analysis, vol. 6. New York: Plenum Press, 1963. p. 231.
[29] Wilchinsky ZW. J Appl Phys 1959;30:792.
[30] Fratini AV, Cross EM, Whitaker RB, Adams WW. Polymer 1986;27:861.
[31] Sauer BB, Hsiao BS. J Polym Sci, Polym Phys 1993;31:917.